Journal of Ceramic Processing Research. Vol. 13, No. 6, pp. 705~712 (2012)

J O U R N A L O F
Ceramic Processing Research

Fabrication and mechanical properties of WC-10 wt.% Co hard materials for a friction stir welding tool application by a spark plasma sintering process

Hyun-Kuk Park[a,b], Hee-Jun Youn[a], Jung-Han Ryu[a], Hyeon-Taek Son[a], Hee-Seon Bang[c], In-Jin Shon[b] and Ik-Hyun Oh[a,*]

[a]*Korea Institute of Industrial Technology (KITECH), Automotive Components Group, 1110-9 Oryong-dong, Buk-gu, Gwang-Ju, 500-480 Korea*

[b]*Division of Advanced Materials Engineering and Research Center of Advanced Materials Development, Chonbuk National University, 664-14 Deokjin-dong 1-ga, Deokjin-gu, Jeonju, Jeonbuk 561-756, Korea*

[c]*Department of Naval Architecture and Ocen Engineering, Chosun University, 375, Seosuk-dong, Dong-gu, Gwangju, 501-759, Korea*

Using the spark plasma sintering process (SPS process), WC-10 wt.%Co hard materials were densified using an ultra fine WC-Co powder. The WC-Co was almost completely dense with a relative density of up to 100% after the simultaneous application of a pressure of 60 MPa and an electric current for 12 minutes almost without any significant change in the grain size. The average grain size of WC that was produced through SPS was about 0.5~0.7 μm. The hardness and fracture toughness at 1200 ^{o}C were about 2068.38 kg/mm^2 and 10.21 MPam$^{1/2}$, respectively. The WC-10 wt.%Co sintered-body was used to give shape to a concave-styled Friction stir weld (FSW) tool. This tool was used to successfully weld mild steel by FSW (SS400). The mechanical properties (micro-hardness, tensile strength, and impact toughness) of the welded mild steel were investigated.

Key words: Spark plasma sintering method, WC-Co, SS400, Friction stir welding, Mechanical property.

Introduction

Friction stir welding (FSW) is a solid-state joining process and is the focus of constant attention in joining low and high temperature strength materials. It was invented by the Welding Institute, UK, in 1991. FSW has appeared as a simple and ecological process. It is a promising and productive welding method that reduces material waste and avoids the radiation and harmful gas emissions usually associated with fusion welding processes [1].

The technique is a variant of friction welding processes. FSW differs from these processes in that it utilizes a rotating tool with a shoulder and a profiled probe that is plunged into the work pieces and traversed along the weld centerline. The most common FSW tools are those used by Megastir co. (USA), PCBN, or Furuya co. (JAPAN), W-Ir or Re. However, these tools are very expensive, brittle, and demand a sensitive processing technique. The FSW tool presented in this study uses tungsten carbide-cobalt hard materials.

Tungsten carbide-cobalt hard materials (WC-Co) are widely used for a variety of applications such as machining, cutting and drilling. Morphologically, they consist of a high volume fraction of the "hard" hexagonal WC phase that is embedded within a soft and tough Co binder phase [2]. These WC-Co hard materials can be densified through liquid phase sintering, and the mechanical properties of these materials depend on their composition and microstructure (especially on the grain size of the carbide phase [3]). Thus, the grain growth of the carbide phase must be controlled during liquid phase sintering. In general, the mechanical properties, such as the hardness, wear resistance, and transverse rupture strength of the composites, increase with a decrease in the WC particle size [4]. Increasing the volume fraction of Co increases the fracture toughness at the expense of the hardness and the wear resistance [5].

The materials used in an FSW tool must have high density, good mechanical properties, and a fine-grained microstructure. The properties of the FSW-tool material determine the performance properties of the welded plate. As such, properties such as density, hardness, fracture toughness, wear resistance, and grain size should be satisfied.

Spark plasma sintering (SPS) is possible at low temperatures and in short amounts of time. This is because the powder surface is activated by applying a high-voltage pulse current between gaps in the powder. One advantage of this process is that a micro structural compact with a high density can be fabricated. Recently, SPS has been studied and applied to the development of FSW-tool materials. Densification by SPS is extremely fast compared to conventional

*Corresponding author:
Tel : +82 62 600 6100
Fax: +82 62 600 6149
E-mail: ihoh@kitech.re.kr

sintering methods in which an external pressure is applied, such as hot pressing (HP) or hot isostatic pressing (HIP). Thus, the sintering temperatures can be lower, which limits the grain growth [6-10].

The goals of this study were to produce dense, ultra-fine WC-10 wt.%Co hard materials in very short sintering times (< 12 minutes) with a large size sintered-body (diameter 65 mm × thickness 30 mm) via the SPS process and then to shape a concave-styled FSW-tool. Additionally, the mechanical properties of the WC hard materials and mild steel (SS400) were investigated.

Experimental procedure

In this study, 99.95% pure tungsten carbide (0.4 ~ 0.5 μm, TaeguTec Ltd., S. Korea) and 99.8% pure cobalt (1.6 μm, Alfa Products, America) powders were used as the raw materials. Fig. 1 shows the FE-SEM images of the raw materials and milled powders that were used. A particle size analyzer was used to examine raw WC and Co materials (Malvern, mastersizer 2000E). The WC and Co particle sizes were 0.2~0.3 μm and 10~20 μm, respectively. Additionally, the average grain sizes of WC and Co were about 0.3 μm and 15 μm with distributions of d(0.1) : 0.129 μm, d(0.5) : 0.199 μm, d(0.9) : 0.384 μm and d(0.1) : 6.413 μm, d(0.5) : 12.098 μm, d(0.9) : 23.844 μm, respectively. The mixed WC and Co powder with a molar ratio of 9 : 1 was milled in a high energy ball mill (planetary mill) at 250 rpm for 10 h. Tungsten carbide balls (6 mm in diameter) were used in a sealed cylindrical stainless steel vial with alcohol. The weight ratio of the balls-to-powder was 10 : 1, and the alcohol-to powder-was 2 : 1. The milling significantly reduced the grain size of the powder. The grain size and the internal strain were calculated using Stokes and Wilson's formula [11]:

$$b = b_d + b_e = k\lambda / (d\cos\theta) + 4\varepsilon\tan\theta \quad (1)$$

where, b is the full width at half-maximum (FWHM) of the diffraction peak after instrumental correction; b_d and b_e are the FWHM for a small grain size and internal stress, respectively; k is a constant (with a value of 0.9); λ is the wavelength of the X-ray radiation; d and ε are the grain size and the internal stress, respectively; and θ is the Bragg angle. The parameters b and bs follow Cauchy's form with the relationship: $B_0 = b + b_s$, where B_0 and b_s are the FWHM of the broadened Bragg peaks and the standard sample's Bragg peaks, respectively. Fig. 2 shows the XRD patterns of the raw materials and the milled WC-10 wt.% Co powder mixture. The FWHM of the milled powder was greater than the raw powders because of the reductions in the internal strain and the grain size. The average grain sizes of the milled WC and Co powders were about 221 and 29 nm, respectively. Additionally, the milled powder exhibited a particle size of about 140 nm and appeared to have a distribution of d(0.1) : 0.062 μm, d(0.5) : 0.094 μm, d(0.9) : 0.141 μm. After milling, the mixed powders were placed in a graphite die (outside diameter, 140 mm; inside diameter, 65 mm; height, 160 mm), and then placed into a spark plasma sintering system that was made by Sumitomo Coal Mining in Japan. A schematic diagram of this method is shown in Fig. 3. The SPS apparatus included a 12 V, 30,000 A DC power suppliy (which provided a pulsed current for 12 millisecond with an off time of 2

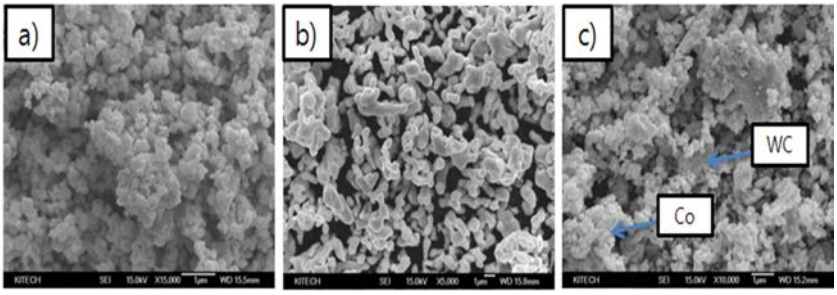

Fig. 1. FE-SEM images of raw materials: a)WC, b) Co and c) milled powder.

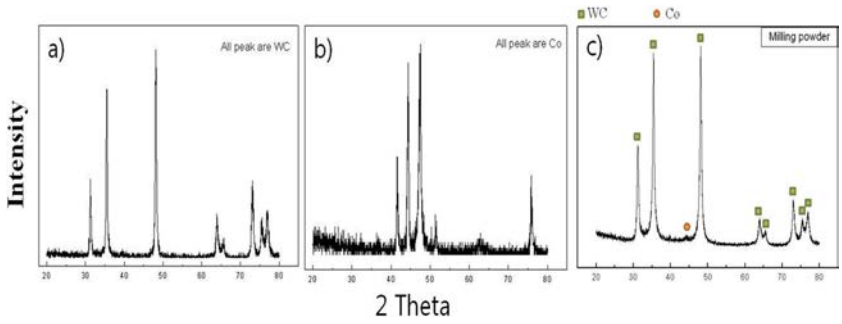

Fig. 2. XRD patterns of WC-10 wt.%Co hard materials: a) WC, b) Co and c) ball milled.

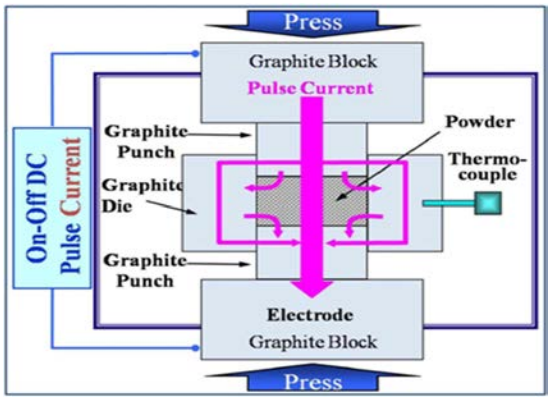

Fig. 3. Schematic diagram of the Spark Plasma Sintering apparatus.

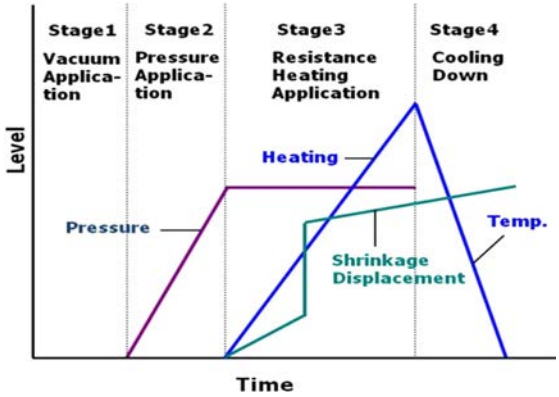

Fig. 4. Schematic representation of the temperature, pressure and shrinkage displacement profile during SPS.

millisecond through the sample and die) and a 300 ton uniaxial press. First, the system was evacuated, and a uniaxial pressure of 60 MPa was applied. Then a pulse current was activated and maintained until the densification rate was negligible, as indicated by the observed shrinkage of the sample. The sample shrinkage was measured in real time using a linear gauge for the vertical displacement in fig. 4. The temperature was measured using a pyrometer that was focused on the surface of the graphite die. The heating rate was approximately 333 K/min during this process. At the end of the process, the current was turned off, and the sample was allowed to cool to room temperature. The entire densification process using the SPS technique consisted of four major control stages, including the chamber evacuation, pressure application, power application, and cool down. This process was carried out under a vacuum of 6 Pa. The relative densities of the sintered samples were measured using the Archimedes density method. Microstructural information was obtained from the product samples, which were polished and etched using Murakami's reagent (5 g $Fe_3(CN)_6$, 5 g NaOH, and 50 ml distilled water), for 30 s at room temperature. The compositional and microstructural analyses of the products were carried out through X-ray diffraction (XRD) and field-emission scanning electron microscopy (FE-SEM).

The hardness was measured by performing indentation tests at a load of 30 kg and a dwell time of 15 s. The carbide grain size, d_{wc}, was obtained using the linear intercept method [12, 13].

Results

The XRD and FE-SEM analyses confirmed that a reaction did not take place and the shrinkage was not significant when a pulsed current was applied to the specimen with a small (thermal) expansion, abruptly increasing at approximately 780. Fig. 5 (a), (b), (c) and

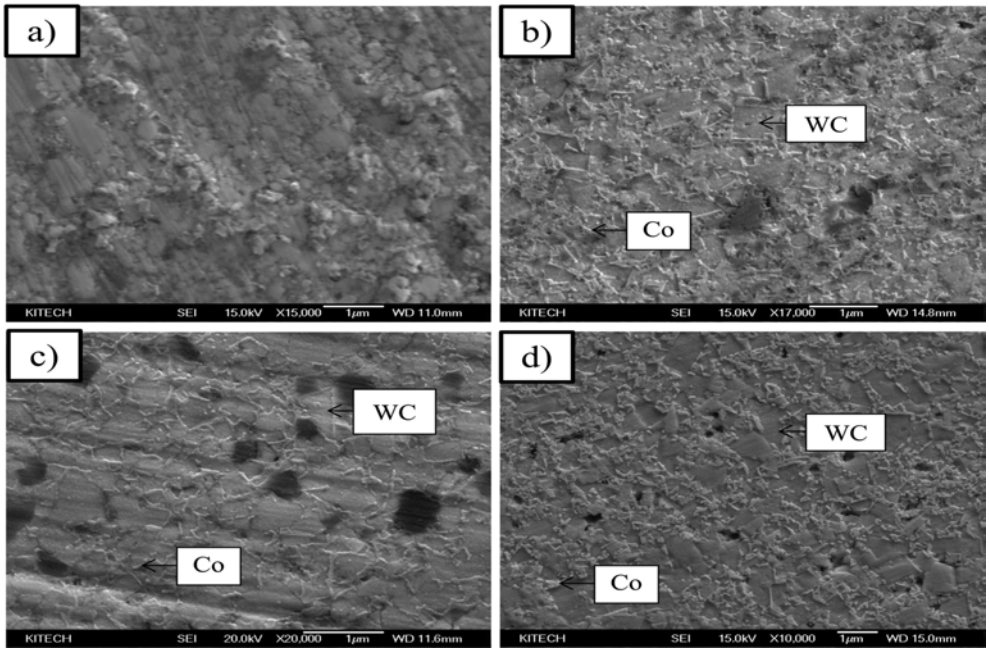

Fig. 5. FE-SEM images of WC-10wt.%Co Sintered-body : a) 900, b) 1000, c) 1100 and d) 1200 under 60 MPa by SPS.

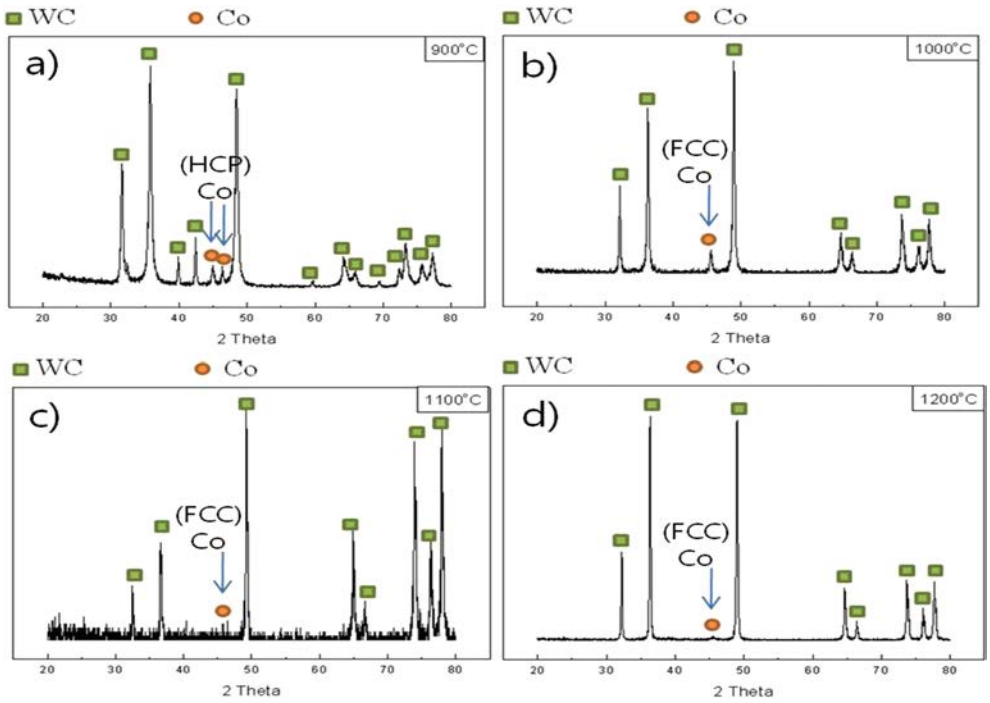

Fig. 6. XRD patterns of WC-10wt.%Co hard materials: a) 900, b) 1000, c) 1100 and d) 1200 under 60 MPa by SPS.

(d) show the FE-SEM (field emission scanning electron microscopy) images of a sample that were heated from 900 to 1200 °C, respectively. Fig. 5 (a) shows an image different from the other images Fig. 5 (b), (c) and (d). Fig. 6 (a) and (b), (C), (d) show the presence of the reactants as separate phases. In Fig. 6 (a), the X-ray diffraction results only exhibited peaks that pertained to the reactants, WC and the hcp crystal structure of Co. However, when the temperature was raised to 1100 °C, the starting powder completely reacted to produce fully dense products. These conclusions were supported by the X-ray diffraction analyses with peaks corresponding to the product phase, including WC and the fcc crystal structure of the Co phase, in Fig. 6 (b), (c) and (d). The solubility limit of tungsten in cobalt is about 10 at.% for the eutectic temperature of 1350 °C and strongly varies with the carbon content. Both tungsten and carbon stabilized the high temperature fcc phase of Co by impeding the martensitic transformation [12]. Therefore, the fcc phase of Co existed at room temperature. For pure WC, only peaks belonging to WC were observed, indicating that no compositional changes took place during sintering. No peaks for the sub-carbide W_2C or any impurity phase are present in Fig. 6 (b), (c) and (d). For the WC-10 wt.% Co cermets, only the WC and Co peaks were observed. In the XRD patterns of the products, a solid solution was not observed because the solid solution peaks overlapped with Co.

Two different methods were used to calculate the grain size (Stokes and Wilson's formula and the linear intercept method). The first expression, which was proposed by Stokes and Wilson's formula, produced an average grain size of about 410 nm for the sintered-body WC [14].

In the second expression, which was proposed by the linear intercept method, the sample surface preparation for the FE-SEM investigations was performed in accordance with the ASTM Method B657 for the metallographic determination of the microstructure in cemented carbides. Accordingly, the surface was polished in three steps. First, the samples were hand-ground on a 120 pm grade diamond grinder in order to remove at least 100 pm of the material. Then a 6 pm grade grinder was used. Finally, the samples were polished using a 1 μm grade diamond paste. The surface was etched using Murakami's reagent for 1 minute at room temperature, then rinsed with alcohol and dried with acetone through ultra sonication in order to identify the WC phase. Fig. 5(c) shows the FE-SEM image of the etched surface of the sample that was heated to 1100 °C at a pressure of 60 MPa. The structural parameters, i.e. the carbide grain size d_{wc} and the mean free path of the binder phase k (the average thickness of the binder phase), were obtained from the boundary intercepts with the test lines on the planar sections. The average number of intercepts per unit length of the test line was determined using the traces of the carbide/cobalt interface, $N_{WC/Co}$, and the carbide/carbide grain boundaries, $N_{WC/WC}$. From these quantities, the average carbide grain size and the mean free path were calculated using the following relationship [11, 12]:

$$d_{WC} = 2V_{WC} / (2N_{WC/WC} + N_{WC/Co}) \quad (2)$$

where, V_{WC} is the carbide volume fraction, and V_{Co} is the binder volume fraction. The average size of about

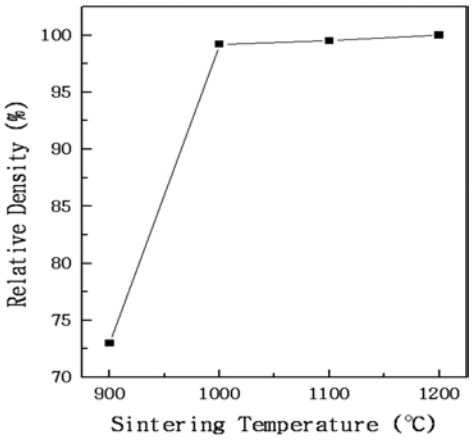

Fig. 7. Relation of relative density and sintering temperature.

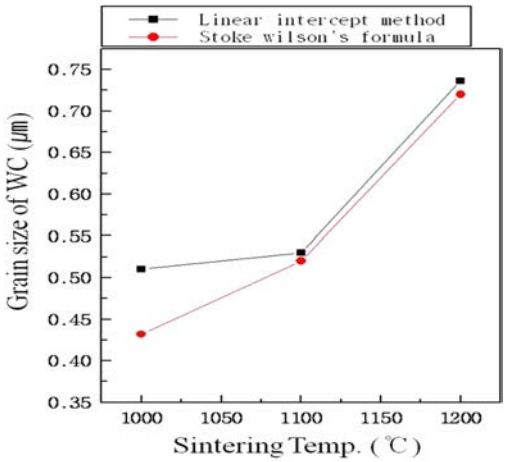

Fig. 8. Relation between WC grain size and sintering temperature.

Table 1. Comparison of the mechanical properties of WC-10 wt.%Co sintered in this study with previously reported values.

Ref.	Binder contents (wt.%)	Relative density (%)	Grain Size (μm)	Hv (Kg/mm^2)	KIC ($MPa \cdot m^{1/2}$)
[1]	6Co	100	0.3	1816	15.1
[13]	10Co	98.2	0.45	1776	10.6
[13]	10Fe	99.7	0.45	1814	10.4
[14]	10Co	99.5	1.9	1333	13.5
[14]	9.6Ni-0.4Co	99.5	1.8	1180	12.5
This Study	WC-10Co	100	0.7	2068	10.2

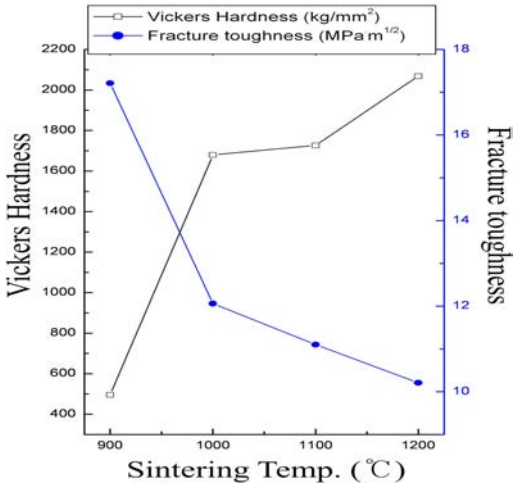

Fig. 9. Variation of vickers hardness and fracture toughness of WC-10wt.% Co under 60 MPa

700 nm for these grains in the nearly fully dense WC-10 wt.% Co composites was determined using the linear intercept method. These two different methods produced similar average grain sizes of 410 and 700 nm, respectively. Thus, a fine structure was obtained without any grain growth during sintering using the SPS method.

This shows that nearly fully dense samples could be obtained by SPS at 1100 ºC, where with conventional vacuum sintering it generally needs about 1400 ºC for 30 minutes. It is obvious that not only the sintering temperature was reduced, but also the sintering time was shortened by SPS. The results prove that SPS is a potential method for fast heating and sintering. Fig. 7 is the relation between the relative density and the sintering temperature. This shows that the densities of the samples increase rapidly with an increase in the sintering temperature to 1000 ºC and then slowly. There is an abnormal phenomenon in the fast sintering of ceramics by SPS, in which the relative density of samples will be up to the maximum at some temperature, but when exceeding this temperature, the relative density of samples will decline. There was no such phenomenon here during sintering cemented carbides by SPS [15-17]. Fig. 8 shows that the WC grain size is from about 500 nm for the sample sintered at 1000 ºC to 720 nm for the sample sintered at 1200 ºC.

The Vickers hardness measurements were taken on the polished sections of the binder WC-10 wt.% Co hard materials using a 30 kgf load at a dwell time of 15 s. At large enough loads, the indentations produced median cracks that emanated from the corners of the indent. The fracture toughness was calculated from the cracks that were produced from the indentations under large loads. The length of these cracks was used to estimate the fracture toughness of the material through the Anstis expression [18].

$$K_{IC} = 0.016(E / H)^{1/2} P / C^{3/2} \quad (3)$$

where, E is the Young's modulus, H is the indentation hardness, P is the indentation load, and C is the trace length of the crack that was measured from the center of the indentation. The modulus was estimated for the rule mixtures with a volume fraction of 0.103 of Co and 0.897 WC using E(Co) = 209 GPa and E(WC) = 696 GPa. The elastic modulus E of WC-10 wt.% Co was about 647.3 GPa. As with the hardness values, the toughness values were derived from the average of five

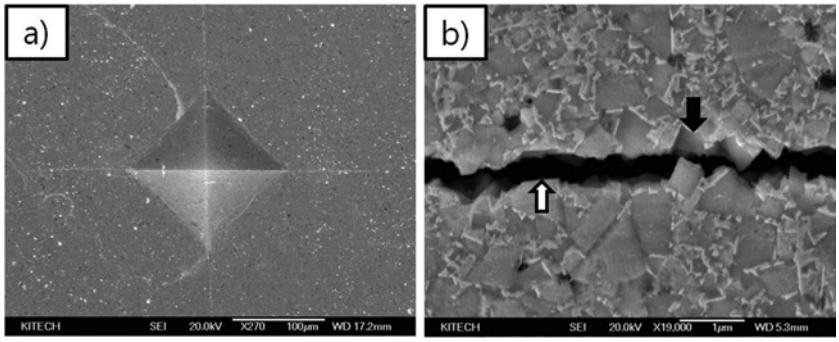

Fig. 10. (a) Vickers hardness indentation and (b) median crack propagation of the sintered WC-10wt.% Co.

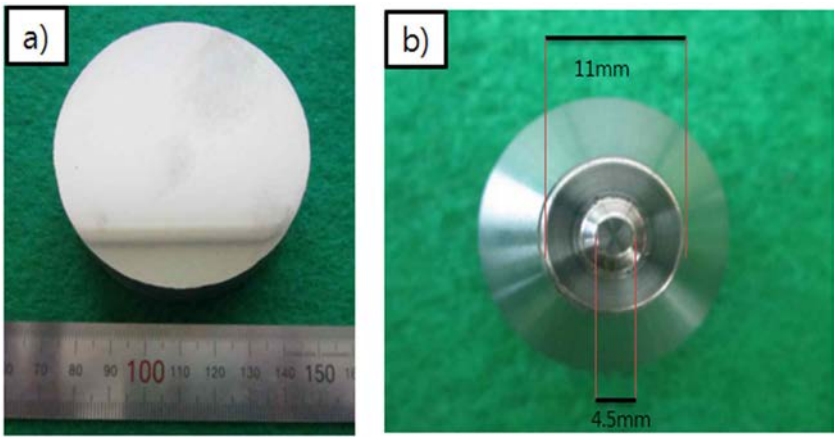

Fig. 11. Images of WC-10wt.% Co hard materials : a) Sintered-body and b) Shape of FSW-Tool

measurements. The calculated hardness and fracture toughness values of sintered WC-10 wt.% Co at 60 MPa and 1200 °C with a WC size of about 720 nm were 2068.38 kg/mm^2 and 10.63 MPa · m$^{1/2}$, respectively. Table 1 shows the calculated structural characteristics of the WC-Co composites, including the hardness and fracture toughness values, from the above formulas, based on the planar section measurements.

Fig. 9 shows the Vickers hardness and fracture toughness of WC-10 wt.% Co as a function of sintering temperature. As expected, the fracture toughness increased and the hardness decreased with increasing temperature.

A typical indentation pattern for the WC-10 wt.% Co composite is shown in Fig. 10 (a). Typically, one to three additional cracks propagated from the indentation corner. A higher magnification view of the indentation median crack in the composite is shown in Fig. 10 (b). This figure shows that the crack propagated along the phase boundary of WC and Co. The crack segments ran both along the WC-Co phase boundaries (white arrows) and through the WC phase itself (black arrows). The Co binder phase is known to prevent crack propagation in the cemented carbide by shielding a stress field in front of the crack tip or by bridging the crack forming ligaments behind the crack tip [21-22].

Fig. 11 (a) shows the WC-10 wt.% Co sintered-body with a diameter and thickness of Ø 65 and 31 mm, respectively. The shape of the fabricated FSW-tool is displayed in Fig. 11 (b), exhibiting a diameter of probe Ø 4.5, height 1.6 mm, and shoulder Ø 11. The fabricated WC-10 wt.%Co tool was used to weld mild steel sheets with dimensions of 1000 mm length × 150 mm width × 2 mm thickness by FSW. The welding conditions and SS400 composition are shown in Table 2.

FSW is a solid state joining method with five steps as shown in Fig. 12 (a). The first step is the plunging period, in which the probe is fully plunged and the shoulder partially plunged into the joint line of the work piece. The second step is the dwell period, during which the tool keeps on rotating at the plunge point. In this step the material around the tool is heated due to the friction between the probe and matrix surfaces caused by the sliding action. Materials around the tool become plasticized as a result of this thermo-mechanical action. The third step is the steady state welding period, during which the rotating tool is traversed along the welding line. This is followed by a second dwell period, which is the fourth step. The fifth and last step is the releasing period. In this step the rotating tool is raised up from the weld line leaving behind a probe cavity in the work piece. Fig. 12 (b) shows the welded joint results of mild steel.

No visible defects were observed at the cross section of the welded joint, as shown by Fig. 13, where AS is the advancing side and RS is the retreating side, the stir zone (SZ) can be seen to contain material that interacts

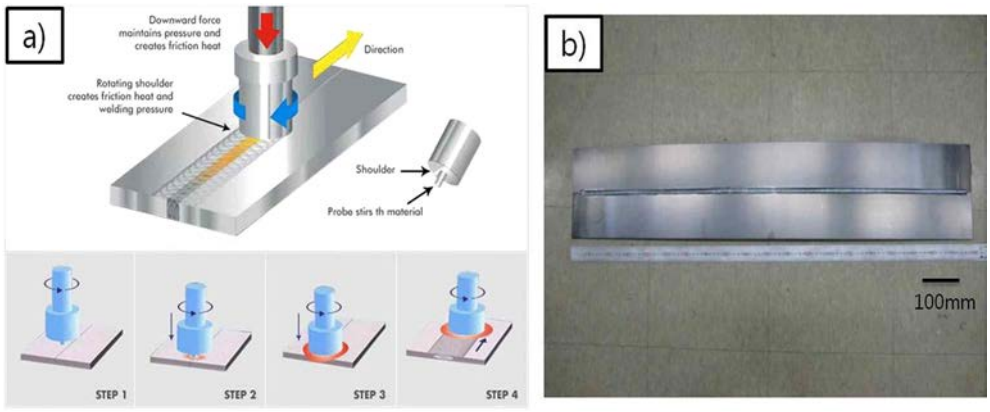

Fig. 12. Schematic diagram of FSW method (a) and welded plate (b).

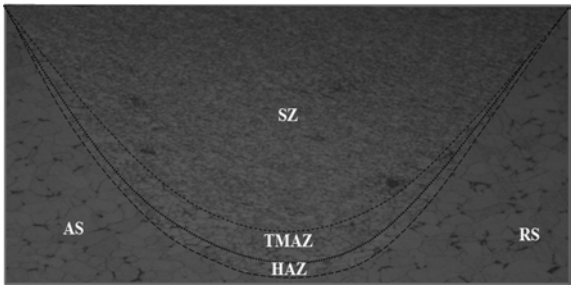

Fig. 13. Macrostructure of friction stir welded SS400.

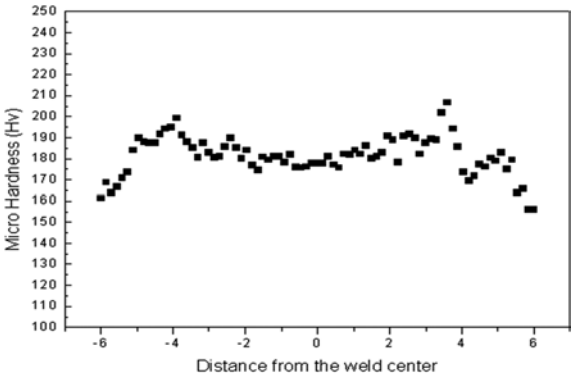

Fig. 14. Micro hardness of friction stir welded SS400.

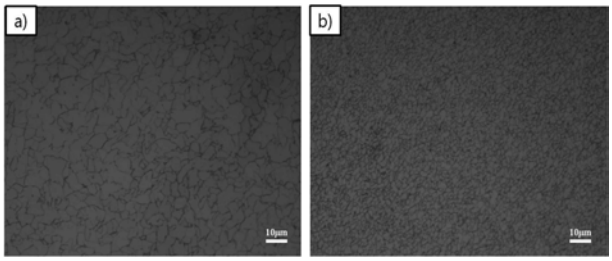

Fig. 15. Images of optical microscope at (a) base metal and (b) Stir zone.

directly with the tool. The dynamically heat affected zone (HAZ) is affected by the heat generated during FSW. The thermo-mechanically affected zone (TMAZ) contains material that interacts indirectly with the tool.

The transverse tensile properties of the FSW joint

Table 2. Welding conditions and SS400 composition.

Mild Steel (SS400)	Chemicl Composition					
	C	Si	Mn	P	S	Fe
	0.14	0.007	0.67	0.01	0.003	Balance
	Tool Size			FSW Condition		
FSW	Probe	Probr Height	FSW-Tool	Rotation Speed		Travel speed
	Ø 4~5	1.6 mm	WC-10 Wt.% Co	600 RPM		6 mm/s

Table 3. Ultimate tensile strength property of welded joints.

Joint Type	Yield Strength (MPa)		Ultimate tensile Strength		Elongation (%)		Joint efficiency (%)
	Replicates	Mean	Replicates	Mean	Replicates	Mean	
BM	299	285	365	354	32	30	-
	274		346		29		
	282		351		30		
FSW	293	297	391	396	20	21	100
	298		396		22		
	302		402		22		

such as yield strength, ultimate tensile strength, and elongation of the joints were evaluated and are presented in Table 3. The ultimate tensile strength and yield strength were seen to be the same as the strength of the base metal, as the failure occurred in the base metal region of the welded joint. The ductility of the SZ was lower than the base metal(BM), as shown in Table 3.

Fig. 14 shows the micro hardness as measured at the mid thickness of the welded joint. The hardness of the as-received base metal is approximately 160 Hv. The hardness of the SZ varies from 170 to 205 Hv.

Fig. 15 displays images of the base metal and top of the SZ as seen by an optical microscope. The grain size of the SZ was smaller than that of the base metal. Therefore, increased strength and hardness were expected due to the

Hall-Patch equation In reality, The micro hardness at the SZ increased and a fracture of the tensile specimens occurred in the base metal region. As a result, weld ability was considered to be 100% satisfactory.

Summary

The WC-10 wt.% Co hard materials were rapidly consolidated using the spark plasma sintering method with ultra fine WC and Co powders. Almost fully dense WC-10 wt.% Co was obtained within 12 minutes. The densification temperature of WC was reduced remarkably through the addition of Co. The grain size of WC was about 500 ~ 700 nm and a nano-structure was obtained without any grain growth during sintering using the SPS process (spark plasma sintering). The fracture toughness and the hardness values of WC-10 wt.% Co were 10.63 MPa · $m^{1/2}$ and 2068.38 kg/mm^2 at 1200 °C under 60 MPa. The fabricated sintered-body is concave shaped to facilitate the FSW-Tool, which has a diameter of probe Ø 4.5 mm, height 1.6 mm, and shoulder Ø 11 mm. The WC-10 wt.% Co tool was used to successfully carry out FSW on 2 mm thick SS400 plates at a rotation speed of 600 RPM and welding traveling speed of 6 mm/s. The tensile strength and hardness of the SZ is seen to be 8% higher than that of the base metal.

References

1. M Enomoto, [J]. Wed lint. 17-5 (2003) 341-346.
2. B.K. Kim, G.H. Ha, D.W. Lee: J Mater Process Technol 63 (1997) 317-321.
3. FL Zhang, CY Wang, M Zhu.: Scripta Mater. 49 (2003) 1123-1128.
4. S.G. Shin: Met. Mater. Int. 6 (2000) 195-201.
5. T Ungar, A Borbely : Nanostruct Mater. 11 (1999) 103-113.
6. M Tokita: Nyn Seramikkasu 10 (1997) 43-54.
7. R Orru, R Licheri, AM Locci, A Cincotti, G Cao: Mater Sci Eng R 63 (2009) 127-287.
8. ZA Munir, U Anselmi-Tamburini, M Ohyanagi: J Mater Sci 41 (2006) 763-77.
9. R Chaim: Mater Sci Eng A 443 (2007) 25-32.
10. W Chen, U Anselmi-Tamburini, JE Garay, JR Groza, ZA Munir: Mater Sci Eng A 394 (2005) 132-8.
11. F.L. Zhang, C.Y. Wang, M. Zhu: Scripta Mater. 49 (2003) 1123-1128.
12. K Jia, TE Fischer, G Gallois: Nanostruct Mater. 10 (1998) 875-891.
13. J.H. Han, D.Y. Kim: Acta Mater. 46 (1998) 2021-2028.
14. H.C. Kim, H.K. Park, I.K. Jung, I.Y. Ko, I.J. Shon: Ceram. Int. 34 (2008) 1419-1423.
15. X. Wang, Y. Xie, H. GUO, O. V. Biest: Rare Met. 25 [3] (2006) 246-252.
16. W. Li, J. Gao, H. Miyamoto, D.L.T. Sebastian: J. Inorg. Mater. 14 [6] (1999) 985-990.
17. J.F. Liu, Z.Y. Fu, H. Wang, D.H. He, Q.J. Zhang: J. Ceram. Soc. 22 [3] (2001) 157-161.
18. GR Anstis, P Chantikul, BR Lawn, DB Marshall: J. Am. Ceram. Soc. 64 (1981) 533-538.
19. H.C. Kim, D.Y. Oh, I.J. Shon: Int. J. Ref. Met. Hard Mater. 22 (2004) 197-203.
20. LS Sigl, HF Fischmeister: Acta Metall. 36 (1988) 887-897.
21. LS Sigl, PA Mataga, BJ Dalgleish, RM McMeeking, AG Evans: Acta Metall. 36 (1988) 945-958.
22. H Engqvist, GA Botton, N Axen, S Hogmark: J. Am. Ceram. Soc. 83 (2000) 2491-2497.